PCCP

ROYAL SOCIETY OF CHEMISTRY

PAPER

Cite this: *Phys. Chem. Chem. Phys.*, 2020, **22**, 14875

Mass spectrometry and computational study of collision-induced dissociation of 9-methylguanine–1-methylcytosine base-pair radical cation: intra-base-pair proton transfer and hydrogen transfer, non-statistical dissociation, and reaction with a water ligand†

Yan Sun,[ab] May Myat Moe[ab] and Jianbo Liu *[ab]

A combined experimental and theoretical study is presented on the collision-induced dissociation (CID) of 9-methylguanine–1-methylcytosine base-pair radical cation (abbreviated as $[9MG{\cdot}1MC]^{\bullet+}$) and its monohydrate ($[9MG{\cdot}1MC]^{\bullet+}{\cdot}H_2O$) with Xe and Ar gases. Product ion mass spectra were measured as a function of collision energy using guided-ion beam tandem mass spectrometry, from which cross sections and threshold energies for various dissociation pathways were determined. Electronic structure calculations were performed at the DFT, RI-MP2 and DLPNO-CCSD(T) levels of theory to identify product structures and map out reaction potential energy surfaces. $[9MG{\cdot}1MC]^{\bullet+}$ has two structures: a conventional structure $9MG^{\bullet+}{\cdot}1MC$ (population 87%) consisting of hydrogen-bonded 9-methylguanine radical cation and neutral 1-methylcytosine, and a proton-transferred structure $[9MG - H]^{\bullet}{\cdot}[1MC + H]^{+}$ (less stable, population 13%) formed by intra-base-pair proton transfer from the N1 of $9MG^{\bullet+}$ to the N3 of 1MC within $9MG^{\bullet+}{\cdot}1MC$. The two structures have similar dissociation energies but can be distinguished in that $9MG^{\bullet+}{\cdot}1MC$ dissociates into $9MG^{\bullet+}$ and 1MC whereas $[9MG - H]^{\bullet}{\cdot}[1MC + H]^{+}$ dissociates into neutral $[9MG - H]^{\bullet}$ radical and protonated $[1MC + H]^{+}$. An intriguing finding is that, in both Xe- and Ar-induced CID of $[9MG{\cdot}1MC]^{\bullet+}$, product ions were overwhelmingly dominated by $[1MC + H]^{+}$, which is contrary to product distributions predicted using a statistical reaction model. Monohydration of $[9MG{\cdot}1MC]^{\bullet+}$ reversed the populations of the conventional structure (43%) *vs.* the proton-transferred structure (57%) and induced new reactions upon collisional activation, of which intra-base-pair hydrogen transfer produced $[9MG + H]^{+}$ and the reaction of the water ligand with a methyl group in $[9MG{\cdot}1MC]^{\bullet+}$ led to methanol elimination from $[9MG{\cdot}1MC]^{\bullet+}{\cdot}H_2O$.

Received 2nd April 2020,
Accepted 18th June 2020

DOI: 10.1039/d0cp01788d

rsc.li/pccp

1. Introduction

Guanine (G) is the most easily oxidizable component among the four DNA nucleobases. For comparison, the oxidation potential (E° *vs.* NHE) is 1.29 V for guanosine, 1.42 V for adenosine, 1.6 V for deoxycytidine, and 1.7 V for thymidine.[1,2] In line with that, guanine has the lowest ionization energy, *i.e.*, adiabatic ionization potential (AIE) is 7.75 eV for guanine, 8.27 eV for adenine, 8.66 eV for cytosine (C), and 8.82 eV for thymine.[3,4] This leads to the facile formation of guanine radical cation ($G^{\bullet+}$) in DNA under one-electron oxidation conditions such as radiolysis,[5,6] laser photolysis,[7,8] electron transfer between metal complexes bound to DNA,[9] and various chemical,[10] electrocatalytic,[11,12] and photosensitized[13,14] oxidation. Pairing guanine with cytosine in a Waston–Crick (WC) base pair further decreases guanine oxidation potential by 0.28–0.34 V.[15,16] Similarly, the AIE of guanine lowers by 0.75–0.78 eV[17,18] whereas that of cytosine raises by 0.58 eV[19] in concurrence with the formation of the guanine–cytosine base pair. As a consequence, the radical cations (holes) which have initially formed on other nucleobases in double-stranded DNA would migrate through the duplex DNA and eventually lead to the more stable guanine radical cations.[6,20]

[a] *Department of Chemistry and Biochemistry, Queens College of the City University of New York, 65-30 Kissena Blvd., Queens, NY 11367, USA. E-mail: jianbo.liu@qc.cuny.edu; Tel: +1-718-997-3271*

[b] *PhD Program in Chemistry, The Graduate Center of the City University of New York, 365 5th Ave., New York, NY 10016, USA*

† Electronic supplementary information (ESI) available: Energies of $[9MG{\cdot}1MC]^{\bullet+}{\cdot}H_2O$ conformers calculated at different levels of theory. Cartesian coordinates for the structures in Fig. 1, 2, 5 and 8. See DOI: 10.1039/d0cp01788d

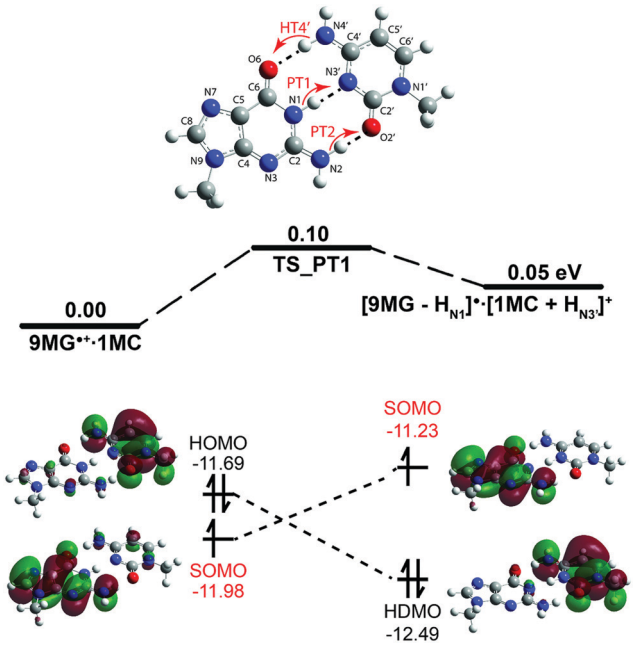

Scheme 1 Stable conformers of $[9MG{\cdot}1MC]^{\bullet+}$, presented with atomic numbering scheme and possible intra-base-pair proton transfer (PT1 and PT2) and hydrogen transfer (HT4′). Relative energies (eV, with respect to the global minimum), and HOMO, HDMO and SOMO were evaluated at ωB97XD/6-311++G(d,p).

Guanine becomes more acidic upon ionization, with the value of pK_a decreasing from 9.4 for guanosine to 3.9 for its radical cation.[5] As a consequence, the $G^{\bullet+}$ in isolation or within single-stranded DNA loses its N1-proton[21] to water (within 56 ns at neutral pH) and forms a neutral $[G - H]^{\bullet}$ radical.[22,23] The $G^{\bullet+}$ within double-stranded DNA, on the other hand, is stabilized through base pairing where the N1-proton (pK_a 3.9)[5] of $G^{\bullet+}$ is shared with the N3 (pK_a 4.3)[24] of C *via* an intra-base-pair proton transfer (PT) equilibrium of $G^{\bullet+}{\cdot}C \rightleftharpoons [G - H]^{\bullet}{\cdot}[C + H]^{+}$.[17,23,25,26] It follows that the guanine–cytosine radical cations $[G{\cdot}C]^{\bullet+}$ are composed of a mixture of $G^{\bullet+}{\cdot}C$ (hereafter referred to as a conventional conformer) and $[G - H]^{\bullet}{\cdot}[C + H]^{+}$ (referred to as a PT conformer). Both conformers maintain a WC structure in the gas phase,[27] as illustrated in Scheme 1 where 9-methylguanine (9MG)–1-methylcytosine (1MC) base-pair radical cation ($[9MG{\cdot}1MC]^{\bullet+}$) was utilized as a model for [deoxyguanosine (dG)·deoxycytidine (dC)]$^{\bullet+}$ (as the methyl mimics the sugar group in a nucleoside). The intra-base-pair PT in guanine–cytosine radical cation not only leads to rare tautomer formation and point mutation,[28] but has significance in the understanding of long-range hole transfer dynamics along the duplex DNA[22,29–34] and in the development of DNA-templated nanowires.[35] It has therefore attracted numerous interests in experimental research (*e.g.*, formation of base-pair radical cations using radiolysis[22,23] and laser photolysis[36,37] followed by ESR,[38,39] transient UV-vis[37,39] and IR[25] detection, and more recently generation of base-pair radical cations using redox charge-separation dissociation of Cu(II)–nucleoside complexes followed by mass spectrometric measurement[27]) and in computational modeling.[17,19,33,40–43]

Collision-induced dissociation (CID) mass spectrometry[44,45] is a useful approach for probing base-pair ion structures and hydrogen bond energies.[46–53] We have previously investigated the intra-base-pair PT in deprotonated 9-methylguanine–cytosine base pair ($[9MG{\cdot}C - H]^{-}$) using the CID mass spectrometry, wherein the $[9MG{\cdot}C - H]^{-}$ anions were colliding with the Xe gas.[52] $[9MG{\cdot}C - H]^{-}$ also consists of a conventional conformation $9MG{\cdot}[C - H]^{-}$ (pairing 9MG with deprotonated cytosine) and a PT conformation $9MG{\cdot}[C - H]^{-}$_PT (formed by an intra-base-pair PT from the N1 of 9MG to the N3 of $[C - H]^{-}$). The two conformers are close in energy and have nearly the same threshold energies for dissociation asymptotes. Therefore, one would have expected similar dissociation product yields from $9MG{\cdot}[C - H]^{-} \rightarrow 9MG + [C - H]^{-}$ *vs.* $9MG{\cdot}[C - H]^{-}$_PT $\rightarrow [9MG - H]^{-} + C$ in the CID of $[9MG{\cdot}C - H]^{-}$. Surprisingly, the product channel of $[9MG - H]^{-} + C$ was found to be overwhelmingly dominant, with its branching ratio being two orders of magnitude higher than a statistical-mechanism-based prediction. Non-statistical product distributions were also observed in the CID of unsubstituted $[G{\cdot}C - H]^{-}$ base pair.[52] Later, we carried out direct dynamics trajectory simulations for the CID of $[G{\cdot}C - H]^{-}$.[54] The trajectories have fully reproduced and thus reinforced the non-statistical CID kinetics of deprotonated guanine–cytosine base pairs, and revealed that the PT conformer dissociates much faster than the conventional conformer.

The discovery of non-statistical dissociation has provided insight into the less intuitive aspects of purine–pyrimidine interactions and base-pair opening. It would be intriguing and informative to determine whether intra-base-pair PT and its entangling with non-statistical dissociation are the characteristic features of guanine–cytosine base pairs regardless of ionization and spin states. With this in mind, herein we report a CID investigation of dry and monohydrated $[9MG{\cdot}1MC]^{\bullet+}{\cdot}(H_2O)_{0,1}$, in which product ion mass spectra and cross sections were measured as a function of collision energy to identify dissociation pathways and determine dissociation threshold energies. Augmented by theoretically calculated reaction potential energy surfaces (PESs), detailed insight was obtained into intra-base-pair reactions, dissociation of guanine–cytosine base-pair radical cations and the effects of explicit hydration.

2. Methods

2.1 Experimental measurement

Collision-induced dissociation tandem mass spectrometry. CID of base-pair radical cations was carried out on a home-built guided-ion-beam tandem mass spectrometer.[52,55] The apparatus consists of an electrospray ionization (ESI) ion source, a radio frequency (rf) hexapole ion guide, a quadrupole mass filter, a rf octopole ion guide surrounded by a scattering cell, a second quadrupole mass filter and a pulse-counting electron multiplier ion detector. $[9MG{\cdot}1MC]^{\bullet+}$ was generated by ESI of Cu(II)–nucleobase complexes, following the methods reported by the O'Hair group[27] and the Bohme group.[56] The ESI solution was prepared in

methanol/water (v : v = 3 : 1) containing 0.25 mM 9MG (chemodex, >98%), 0.25 mM 1MC (enamine, 95%) and 0.25 mM $Cu(NO_3)_2$ (alfa aesar, >99.999%). The solution was sprayed into the ambient atmosphere through an electrospray needle at a flow rate of 0.06 mL h^{-1}. The electrospray needle was held at 2.35 kV relative to the ground. Positively charged droplets entered the source chamber of the mass spectrometer through a pressure-reducing desolvation capillary. The capillary was biased at 94 V and heated to 206 °C, so that liquid aerosols underwent desolvation in the capillary and converted to a mixture of gas-phase $[Cu^{II}(9MG)_n(1MC)_{4-n}]^{\bullet 2+}$ complexes[27] in the source chamber. The source chamber was evacuated to a pressure of 1.7 τ. A skimmer with an orifice of 1.5 mm is located 3 mm away from the capillary exit, separating the source chamber and the hexapole ion guide. The skimmer was biased at 10 V relative to ground. The electrical field between the capillary exit and the skimmer prompted CID of $[Cu^{II}(9MG)_n(1MC)_{4-n}]^{\bullet 2+}$ with background gas, of which $[9MG{\cdot}1MC]^{\bullet +}$ was formed *via* redox charge-separation-induced dissociation of $[Cu^{II}(9MG)_n(1MC)_{4-n}]^{\bullet 2+}$.[27] Monohydrated $[9MG{\cdot}1MC]^{\bullet +}{\cdot}H_2O$ was generated in a similar manner as $[9MG{\cdot}1MC]^{\bullet +}$ except that the ESI solution was prepared in a 2 : 1 methanol/water mixture, the desolvation capillary was heated to 155 °C, and the skimmer was biased at 13.7 V.

Base-pair radical cations were passed into the hexapole at the pressure of 24 mτ. Interaction of ions with the background gas within the hexapole led to ion collisional focusing[57] and thermalization to ~310 K. Ions subsequently passed into the first quadrupole mass filter for selecting base-pair radical ions of specific mass-to-charge ratio (m/z). The mass-selected base-pair radical ions were injected into the octopole ion guide which trapped ions in the radial direction. The octopole was surrounded by a 10 cm scattering cell which was filled with Xe (Spectral Gases, 99.995%) or Ar (T.W. Smith, >99.5%). The cell pressure was controlled at 0.01 mTorr using a leak valve and monitored using a MKS Baratron capacitance manometer. Under these conditions, base-pair radical cations underwent at most a single collision with rare gas.

In addition to rf voltages, DC bias voltage of variable polarity and amplitude was applied to the octopole ion guide. The DC voltage allowed precise control over the kinetic energy of ions in the laboratory frame (E_{lab}), thereby setting the collision energy (E_{col}) between the ions and the collision gas in the center-of-mass frame. That is $E_{col} = E_{lab} \times m_{neutral}/(m_{ion} + m_{neutral})$, where $m_{neutral}$ and m_{ion} are the masses of neutral collision gas and reactant ion, respectively. E_{col} represents the energy available to the system for reactions. CID was measured at an E_{col} range of 0.05–7 eV. Fragment ions and the remaining base-pair reactant ions drifted to the end of the octopole and finally were mass analyzed by the second quadrupole and counted by the electron multiplier.

Ion beam intensities were 6×10^4 count per s for $[9MG{\cdot}1MC]^{\bullet +}$ and 1.4×10^4 count per s for $[9MG{\cdot}1MC]^{\bullet +}{\cdot}H_2O$. Initial kinetic energies of the ion beam were set at 0.8 eV. The energy spreads of the ion beam were controlled to be less than 0.6 eV by a combination of collisional dumping in the hexapole and narrowing the collection radius of the ion beam at the exit of the first quadrupole. Product cross sections were calculated from the ratios of reactant and product ion intensities, the collision gas pressure in the scattering cell and the effective length of the scattering cell. Each measurement was repeated four times, from which the experimental uncertainty was determined.

Measurement of base-pair dissociation thresholds. Due to the kinetic energy spread and the internal energy of the primary ion beam, the cross sections of base-pair dissociation product ions rise from zero before true dissociation thresholds (E_0). To extract an accurate value of E_0, a modified line-of-centers (LOC) model[58–61] was assumed for the E_{col} dependence of "true" cross section $\sigma(E_{col})$:

$$\sigma(E_{col}) = \sigma_0 \frac{(E_{col} + E_{vib} + E_{rot} - E_0)^n}{E_{col}} \quad (1)$$

where σ_0 is an energy-independent scaling factor, E_{vib} and E_{rot} are reactant vibrational and rotational energies, E_0 is as defined above, and n is a fitting parameter used to adjust the slope of $\sigma(E_{col})$. It was assumed that, at the energies near E_0, at least some of the collisions are completely inelastic so that E_{col} is all converted to internal energy, and E_{col}, E_{vib} and E_{rot} have the same effects in driving reactions. These assumptions were verified in the threshold CID of deprotonated guanine–cytosine base pairs[52] and of many other ions.[60]

$\sigma(E_{col})$ was then convoluted with experimental broadening and various kinetic factors using two different approaches. The first approach modeled multiple product channels simultaneously by incorporating statistical inter-channel competition. This was done using an ion-molecular reaction analysis software Crunch developed by Armentrout, Ervin and co-workers.[62–77] In the fitting, the total CID cross section (σ_{total}) was divided among different product channels such that individual product cross section $\sigma_i = (k_i/k_{total}){\cdot}\sigma_{total}$, where the ratio of rate constant k_i/k_{total} was calculated in a statistical manner and induced coupling between product channels in collisional excitation.[45,60] The second approach was to fit individual product channels independently; and a Monte Carlo program developed by Anderson and co-workers[78] was used to sample 100 000 collisions of base-pair radical cations with inert gas at each E_{col}. These collisions simulated the distributions of ion beam and target gas velocities and ion E_{vib} and E_{rot}.

In both fitting approaches, a Maxwell–Boltzmann velocity distribution at 300 K was used for collision gas atoms. The kinetic energy spread of the $[9MG{\cdot}1MC]^{\bullet +}$ ion beam was 0.6 eV. Due to the large size of $[9MG{\cdot}1MC]^{\bullet +}$, a kinetic shift was expected in the near-threshold collisions; that is E_{col} in excess of the dissociation limit was required to produce dissociation within the experimental time scale (~500 μs).[67] To this end, a Rice–Ramsperger–Kassel–Marcus (RRKM, see below)[79] model was included in the fitting to decide whether each collision led to detectable dissociation. A leveling-off collision energy was used in the fitting so that $\sigma(E_{col})$ would reach a plateau at high E_{col}. The rising curvature of $\sigma(E_{col})$ depends sensitively on E_0 and n, and their values were adjusted until the convoluted $\sigma(E_{col})$ reached the best agreement with the experiment.

2.2 Computational modeling

Conformers of [9MG·1MC]$^{\bullet+}$. Prior to reaction PES and kinetics calculations, we needed to identify various conformations of [9MG·1MC]$^{\bullet+}$ and ensure that the lowest-energy conformer is used as the starting geometry in theoretical modeling. Feketeová *et al.*[27] reported a combined infrared multiphoton dissociation (IRMPD) spectroscopy measurement and M06-2X/6-31+G(d,p) calculation of the [dG·dC]$^{\bullet+}$ radical ion in the gas phase. Using [dG·dC]$^{\bullet+}$ conformations as a guide and taking into account other types of tautomerization, we identified 14 conformers for gas-phase [9MG·1MC]$^{\bullet+}$ within an energy range of 1.5 eV. Our conformation search was carried out at the ωB97XD/6-311++G(d,p) level of theory.[80] The ωB97XD functional mitigates self-interaction errors and improves the orbital descriptions of ionized states.[43] Calculations were accomplished using Gaussian 09.[81] Basis set superposition error[82] was less than 0.05 eV and thus would not change the order of stability of these conformers. The structures and enthalpies (ΔH at 298 K, relative to the global minimum) for all 14 conformers are summarized in Fig. 1. Their Cartesian coordinates are provided in the ESI.† These conformers involve intra-base-pair PT, intra-base-pair hydrogen transfer (HT), keto–enol isomerization as well as unnatural base pairing.

The global minimum structure [9MG·1MC]$^{\bullet+}$_1 is a conventional WC base pair. The second lowest-energy structure [9MG·1MC]$^{\bullet+}$_2, with energy lying at 0.05 eV higher than [9MG·1MC]$^{\bullet+}$_1, forms by PT from N1 of 9MG to N3 of 1MC in [9MG·1MC]$^{\bullet+}$_1. [9MG·1MC]$^{\bullet+}$_1 and 2 account for 87% and 13% of the gas-phase [9MG·1MC]$^{\bullet+}$ ion beam, respectively; and the other conformers are negligible. In the remainder of this paper, the two major conformers are referred to as 9MG$^{\bullet+}$·1MC and [9MG − H]$^{\bullet}$·[1MC + H]$^{+}$.

Note that, intra-base-pair HT from the N4 of 1MC to O6 of 9MG (referred to as HT4′) was found in [9MG·1MC]$^{\bullet+}$_9. HT4′ may occur in high-energy collisions, producing a protonated [9MG + H]$^{+}$ moiety. Efforts were made to locate the base-pair structures corresponding to the intra-base-pair PT from 9MG N2–H to 1MC O2 (*i.e.* PT2) and the structures corresponding to concurrent PT from 9MG to 1MC and HT from 1MC to 9MG (*i.e.* PT1 + HT4′ or PT2 + HT4′), but all such starting geometries converged to 9MG$^{\bullet+}$·1MC or [9MG − H]$^{\bullet}$·[1MC + H]$^{+}$.

Conformers of [9MG·1MC]$^{\bullet+}$·H$_2$O. Initial geometries of monohydrated base-pair radical cations were obtained by adding a water to all possible hydration sites in 9MG$^{\bullet+}$·1MC and [9MG − H]$^{\bullet}$·[1MC + H]$^{+}$, and then fully optimized at the ωB97XD/6-311++G(d,p) level of theory. The converged monohydrated structures are depicted in Fig. 2 with their formation ΔH (relative to the global minimum), hydration enthalpies ($\Delta H_{\text{hydration}} = \Delta H_{\text{monohydrate}} - \Delta H_{\text{dry ion}} - \Delta H_{\text{water}}$) and populations at 298 K indicated in parentheses. Their Cartesian coordinates are available in the ESI.† To affirm the relative stabilities of these monohydrated structures, their energies were re-evaluated at several other levels of theory and the results have shown a nearly perfect agreement (see Table S1 in the ESI†).

The hydration energy of [9MG·1MC]$^{\bullet+}$ arises largely from a charge–dipole interaction and the interaction of water with cytosine yields a comparable $\Delta H_{\text{hydration}}$ as that with guanine.[18]

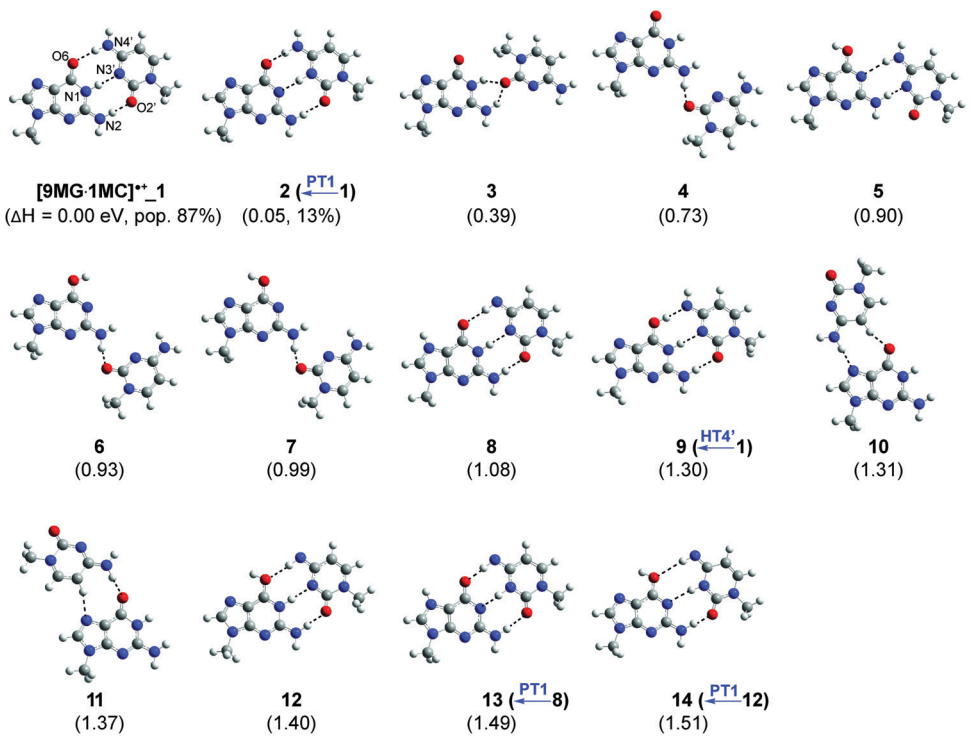

Fig. 1 Stable conformers of [9MG·1MC]$^{\bullet+}$. Dashed lines indicate hydrogen bonds. Relative formation enthalpies (ΔH, eV, with respect to global minimum) and thermal populations were calculated at 298 K using ωB97XD/6-311++G(d,p).

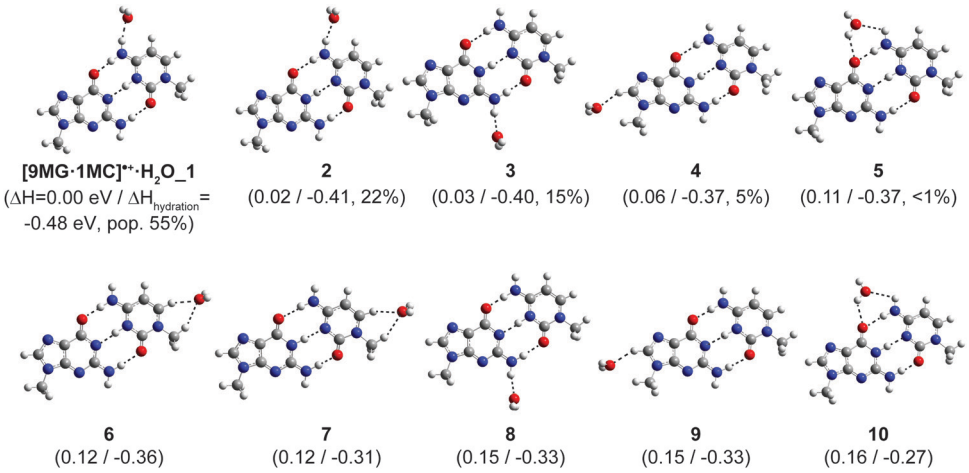

Fig. 2 Stable conformers of $[9MG{\cdot}1MC]^{\bullet+}{\cdot}H_2O$. Dashed lines indicate hydrogen bonds. Relative formation enthalpies (ΔH with respect to global minimum, eV), hydration enthalpies ($\Delta H_{hydration}$, eV) and thermal populations were calculated at 298 K using ωB97XD/6-311++G(d,p).

Of the four lowest-energy monohydrates in Fig. 2, $[9MG{\cdot}1MC]^{\bullet+}{\cdot}H_2O\_1$ (population = 55%) and $[9MG{\cdot}1MC]^{\bullet+}{\cdot}H_2O\_2$ (22%) are formed by attaching a water to the cytosine N4–H in $[9MG - H]^{\bullet}{\cdot}[1MC + H]^{+}$ and in $9MG^{\bullet+}{\cdot}1MC$, respectively; and $[9MG{\cdot}1MC]^{\bullet+}{\cdot}H_2O\_3$ (15%) and $[9MG{\cdot}1MC]^{\bullet+}{\cdot}H_2O\_4$ (5%) are formed by attaching a water to the guanine N2–H and C8–H in $9MG^{\bullet+}{\cdot}1MC$, respectively. The hydration motifs of $[9MG{\cdot}1MC]^{\bullet+}$ resemble those of the unsubstituted $[G{\cdot}C]^{\bullet+}$,[18] except that in $[G{\cdot}C]^{\bullet+}$ guanine N9–H and cytosine N1–H represent the two strongest hydration sites followed by cytosine N4–H and then guanine N2–H. Since guanine N9–H and cytosine N1–H are substituted by methyl in $[9MG{\cdot}1MC]^{\bullet+}$, cytosine N4–H and guanine N2–H now become the two most favorable sites.

An intriguing finding is that the relative stabilities of base-pair radical cation conformers are switched by hydration. The PT structure becomes more stable than the conventional one, as demonstrated by $[9MG{\cdot}1MC]^{\bullet+}{\cdot}H_2O\_1$ *vs.* $[9MG{\cdot}1MC]^{\bullet+}{\cdot}H_2O\_2$. This agrees with previous findings in $[G{\cdot}C]^{\bullet+}$ with a single[41] and eleven waters,[40,42] in both of which the solvated $[G - H]^{\bullet}{\cdot}[C + H]^{+}$ conformer was found to be more stable than the solvated $G^{\bullet+}{\cdot}C$. In the following discussion, the two dominating monohydrated structures $[9MG{\cdot}1MC]^{\bullet+}{\cdot}H_2O\_1$ and 2 are designated as $[9MG - H]^{\bullet}{\cdot}[1MC + H]^{+}{\cdot}H_2O$ and $9MG^{\bullet+}{\cdot}1MC{\cdot}H_2O$, respectively.

Reaction PESs. The analysis of conformer energies and populations in the gas phase have revealed that $9MG^{\bullet+}{\cdot}1MC$ and $[9MG - H]^{\bullet}{\cdot}[1MC + H]^{+}$ dominated the unhydrated reactant ion beam, while $9MG^{\bullet+}{\cdot}1MC{\cdot}H_2O$ and $[9MG - H]^{\bullet}{\cdot}[1MC + H]^{+}{\cdot}H_2O$ represented the main compositions of the monohydrated reactant ion beam. Accordingly, calculations of reaction PESs were initiated at $9MG^{\bullet+}{\cdot}1MC$ and $[9MG - H]^{\bullet}{\cdot}[1MC + H]^{+}$ for the unhydrated system and at $9MG^{\bullet+}{\cdot}1MC{\cdot}H_2O$ and $[9MG - H]^{\bullet}{\cdot}[1MC + H]^{+}{\cdot}H_2O$ for the hydrated one. All stable structures and transition states (TSs) in the PESs were optimized at the ωB97XD/6-311++G(d,p) level of theory. TSs were verified as first-order saddle points, and the vibrational mode associated with an imaginary frequency corresponds to the anticipated reaction pathway. Intrinsic reaction coordinate calculations were carried out to substantiate reactant/product minima connected through the TSs.

Reaction PESs were further validated by single-point energy calculations at ωB97XD/aug-cc-PVQZ, B3LYP/aug-cc-PVQZ, the resolution of identity Møller–Plesset procedure (RI-MP2)/aug-cc-pVTZ (which provides accurate description of hydrogen bonds),[83,84] and the domain based local pair-natural orbital coupled-cluster method with single-, double- and perturbative triple excitations DLPNO-CCSD(T)/aug-cc-pVTZ (which further improves the energy accuracy of base-pair interactions).[85] Electronic energies at these levels of theory were calculated using ORCA 4.0.1.[86] Reaction enthalpies at each level of theory were obtained by the summation of the electronic energies calculated at the specified level, and the zero point energies (ZPEs, scaled by 0.975[87]) and 298 K thermal corrections calculated at ωB97XD/6-311++G(d,p).

RRKM kinetics modeling. The transition-state-based RRKM theory[79] was employed to simulate statistical reaction kinetics. The fundamental assumption in the RRKM model is that energy is randomized and distributed statistically among all of the energetically accessible states in the system, and the rate of a particular dissociation process is proportional to the total number of energetically accessible states at the TS.[88,89] As a consequence, statistical reactions occur *via* minimum-energy pathways, as the density of states is highest for such pathways.[90] RRKM rate constants were calculated as:[91]

$$k_{\mathrm{diss}}(E,J) = \frac{d}{h}\frac{\sum_{K=-J}^{J} G\left[E - E_0 - E_{\mathrm{r}}^{\dagger}(J,K)\right]}{\sum_{K=-J}^{J} N\left[E - E_{\mathrm{r}}(J,K)\right]} \qquad (2)$$

where d is the reaction path degeneracy, G is the sum of accessible states from 0 to $E - E_0 - E_{\mathrm{r}}^{\dagger}$ at the TS, N is the energized reactant's density of states, E is the system energy, E_0 is the unimolecular dissociation threshold, E_{r} and $E_{\mathrm{r}}^{\dagger}$ are the

rotational energies for the reactant and the TS, J is the angular momentum quantum number, and K is the rotation quantum number.

To determine the values of J and E_r for the collisionally activated $[9MG{\cdot}1MC]^{\bullet+}$, direct dynamics trajectories[92] were calculated for the collisions of $[9MG{\cdot}1MC]^{\bullet+}$ with Xe at different E_{col}, with the initial conditions generated by the Venus program[93,94] to mimic the CID experiment. The trajectories were integrated using Gaussian 09, with forces calculated at the B3LYP/6-31G level of theory. J and E_r^- of $[9MG{\cdot}1MC]^{\bullet+}$ were calculated as $J = \vec{r} \times \vec{p}$ and $E_r^- = J^2/2I$ where I is the momentum of inertia. K was treated as active in eqn (2), so that all $(2J + 1)$ K-levels were counted in $k_{diss}(E,J)$. Calculation of k_{diss} was done with the RRKM program of Zhu and Hase[95] using its direct state count algorithm. Reaction energetics, vibrational frequencies and moments of inertia of the reactants and the TSs were obtained from the ωB97XD/6-311++G(d,p) results.

3. Results and discussion

3.1 CID of $[9MG{\cdot}1MC]^{\bullet+}$

Products, cross sections and dissociation thresholds for $[9MG{\cdot}1MC]^{\bullet+}$ + Xe. We started by first measuring the CID of $[9MG{\cdot}1MC]^{\bullet+}$ with Xe over an E_{col} range of 0.1–6.0 eV. Fig. 3a presents a representative product ion mass spectrum measured at E_{col} = 3.0 eV. The detection of both $9MG^{\bullet+}$ (m/z 165) and $[1MC + H]^+$ (m/z 126) in product ions has confirmed that $[9MG{\cdot}1MC]^{\bullet+}$ exists as a mixture of $9MG^{\bullet+}{\cdot}1MC$ and $[9MG - H]^{\bullet}{\cdot}[1MC + H]^+$ in the gas phase. The ωB97XD/6-311++G(d,p)-calculated dissociation threshold energies are:

$$9MG^{\bullet+}{\cdot}1MC \rightarrow 9MG^{\bullet+} + 1MC \quad \Delta H = 2.00\ \text{eV} \qquad (3)$$

$$[9MG - H_{N1}]^{\bullet}{\cdot}[1MC + H_{N3'}]^+ \rightarrow [9MG - H_{N1}]^{\bullet} + [1MC + H_{N3'}]^+ \quad \Delta H = 2.00\ \text{eV} \qquad (4)$$

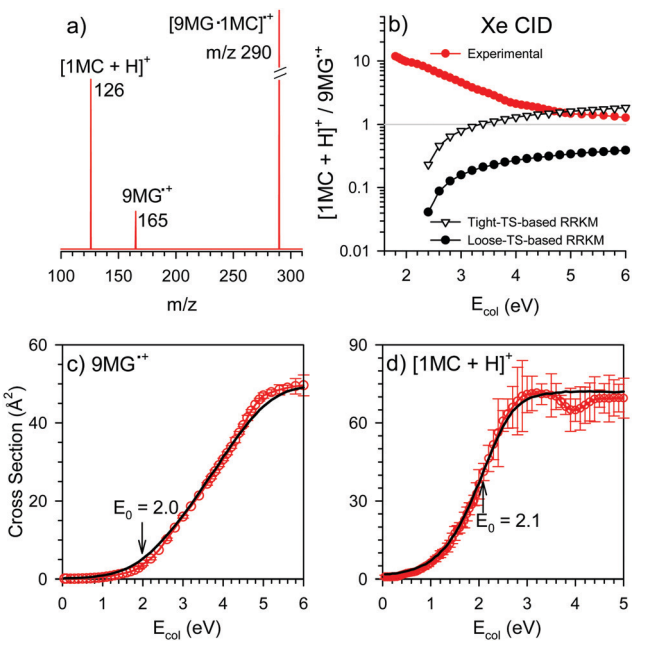

Fig. 3 CID results of $[9MG{\cdot}1MC]^{\bullet+}$ with Xe. (a) CID product ion mass spectrum measured at E_{col} = 3.0 eV, (b) comparison of experimental and RRKM product ion branching ratios as a function of E_{col}, and (c and d) product ion cross sections of $9MG^{\bullet+}$ and $[1MC + H]^+$ where circled points are experimental data and black curves are LOC fits as discussed in the text.

The product branching ratio of $[1MC + H]^+/9MG^{\bullet+}$ was measured as a function of E_{col} and plotted as red circles in Fig. 3b. The branching ratio raises up to 12 at E_{col} = 1.8 eV, decreases with increasing E_{col} and approaches a plateau of 1.2 at $E_{col} > 5.0$ eV. Such results are in contradiction to statistical product distributions expected from the higher population (87%) and the same dissociation threshold (2.00 eV) of $9MG^{\bullet+}{\cdot}1MC$ *vs.* those (13% and 2.00 eV) of $[9MG - H]^{\bullet}{\cdot}[1MC + H]^+$. This contradiction confirms that the guanine–cytosine base-pair radical cations indeed bear non-statistical dissociation behavior as their deprotonated analogues.

Fig. 3c and d present the product ion cross sections of $9MG^{\bullet+}$ and $[1MC + H]^+$, respectively, where the error bars were calculated from the 4 sets of data measured under the same conditions. The cross sections of both product ions increase with E_{col} and seem to approach maxima at high energies. The long range interaction between the base-pair radical cation and the inert gas is negligible, thus their collision cross section could be estimated using a hard-sphere model.[59] The orientation-averaged hard-sphere collision cross section (σ_{HS}) is 130 Å^2 for $[9MG{\cdot}1MC]^{\bullet+}$ + Xe and 120 Å^2 for $[9MG{\cdot}1MC]^{\bullet+}$ + Ar. At sufficiently high E_{col}, every collision is expected to result in dissociation; therefore, the total CID cross section should approach σ_{HS} and become independent of E_{col}. The fact that the sum of $9MG^{\bullet+}$ and $[1MC + H]^+$ cross sections indeed approaches σ_{HS} at 5.0 eV and levels off afterwards confirms that we were able to capture nearly all Xe-induced CID product ions. It is to be noted that the product cross section of $[1MC + H]^+$ stops to increase at 3 eV; whereas that of $9MG^{\bullet+}$ continues to increase till 6 eV. This is more clearly demonstrated by the E_{col}-dependence product branching ratio in Fig. 3b. Albeit that the absolute cross section of $[1MC + H]^+$ is always larger than that of $9MG^{\bullet+}$, $[1MC + H]^+$ is becoming less overwhelming with increasing E_{col}.

To determine the base-pair dissociation thresholds from the experiment, the E_{col}-dependent product ion cross sections were fitted using the two approaches described in Section 2.1, *i.e.*, fit the two product channels simultaneously by incorporating statistical competition *vs.* fit each of the two channels independently. It turned out that the statistical treatment of inter-channel competition resulted in a much lower E_0 for the product channel of $[9MG - H]^{\bullet} + [1MC + H]^+$ than that for $9MG^{\bullet+}$ + 1MC (as the $[1MC + H]^+$ cross section rises more quickly and levels out earlier), which is inconsistent with their dissociation thresholds calculated using various theories (see below). It is not surprising that a statistical treatment failed to reproduce the dissociation energies as the two dissociation

channels do not originate from one single structure of energized base pair.

The black plots in Fig. 3c and d show the independently simulated $\sigma(E_{col})$ for the two CID channels. The best fit E_0 is 2.0 eV (with $n = 2$, $\sigma_0 = 50$ Å^2 and leveling-off energy at 5.6 eV) for $9MG^{\bullet+}{\cdot}1MC \rightarrow 9MG^{\bullet+} + 1MC$ and 2.1 eV (with $n = 2$, $\sigma_0 = 75$ Å^2 and leveling-off energy at 5.6 eV) for $[9MG - H]^{\bullet}{\cdot}[1MC + H]^{+} \rightarrow [9MG - H]^{\bullet} + [1MC + H]^{+}$. The experimental E_0 values are in a good agreement with the calculated dissociation energies. In both fitting, $n = 2.0$ was required to reproduce the concave-up (quadratic) increase of cross section with E_{col}. In the LOC-based model, an orientation-dependent activation barrier often results in a quadratic ($n = 2$) threshold law.[59] For base-pair dissociation, E_0 is not angle-dependent, but the collisional activation is anisotropic and the Xe collision towards the base-pair hydrogen-bond groove might be most effective. This would lead to angle-dependent CID probability, *i.e.* a steric factor. A similar quadratic threshold behavior was observed in the CID cross sections of deprotonated guanine–cytosine base pairs with Xe.[52]

$[9MG{\cdot}1MC]^{\bullet+}$ + Ar. Similar to what was observed in the Xe-induced collisions, the CID products of $[9MG{\cdot}1MC]^{\bullet+}$ + Ar are dominated by $[1MC + H]^{+}$. Fig. 4a presents the product branching ratio of $[1MC + H]^{+}/9MG^{\bullet+}$ measured in the Ar-induced CID, and Fig. 4b and c present the cross sections for the two product channels.

Because our primary interest is in comparing the threshold behaviors for different collision gases, we generated a set of fits for Ar-induced CID cross sections by fixing the n value at 2.0 that gave the best fits for Xe-induced CID and leaving E_0 as the only adjustable parameter. The two product cross sections were fit independently and on the basis of how well convoluted $\sigma(E_{col})$ matched the experimental data at near-threshold E_{col}. The best fit E_0 for the Ar-induced CID is 2.6 eV for both $9MG^{\bullet+}$ and $[1MC + H]^{+}$. These values are 0.5–0.6 eV higher than those for the Xe-induced CID; therefore, it would be more appropriate to take these values as the "product ion appearance energies" with the experimental broadening corrected for. The Ar-CID results indicate that there were no Ar-induced collisions which has 100% translational-to-internal energy transfer ($T \rightarrow E_{internal}$), even near the threshold. To explain these results, we may view CID of $[9MG{\cdot}1MC]^{\bullet+}$ as two steps: $[9MG \cdot 1MC]^{\bullet+}$ + rare gas(Rg) $\rightarrow [9MG \cdot 1MC]^{\bullet+}{\cdot}$ Rg(a transient collision complex) $\xrightarrow{\text{dissociation}} [9MG \cdot 1MC]^{\bullet+*}$ (excited base pair) + Rg, followed by unimolecular dissociation of $[9MG{\cdot}1MC]^{\bullet+}*$. The nature of the $[9MG{\cdot}1MC]^{\bullet+}{\cdot}$Rg complex may be impulsive[96] or statistically behaved.[45,60,97] If the $[9MG{\cdot}1MC]^{\bullet+}{\cdot}$Rg complex can live relatively long for sufficient energy randomization before its decomposition (*i.e.* decompose statistically), most of the excitation energy is left in the internal modes of $[9MG{\cdot}1MC]^{\bullet+}*$ (as Rg is atomic). The differences between Xe and Ar-induced CID can be rationalized in this context, on the basis of their polarizabilities and collision times.[45,60,97] First, among the stable rare gases, Xe has the largest mass and highest polarizability and therefore binds most strongly to ions, which allows $T \rightarrow E_{internal}$ in the most efficient manner possible. Secondly, at the same E_{col}, the $[9MG{\cdot}1MC]^{\bullet+}$ + Xe system has a lower E_{lab} than $[9MG{\cdot}1MC]^{\bullet+}$ + Ar and consequently has relatively longer collision time available for $T \rightarrow E_{internal}$. These properties helped assure a more statistical dissociation of $[9MG{\cdot}1MC]^{\bullet+}{\cdot}$Xe. Indeed, we have found in a number of systems that Ar was an inefficient collider, and Ar-induced CID was not observed until E_{col} far exceeded dissociation thresholds.[61,98]

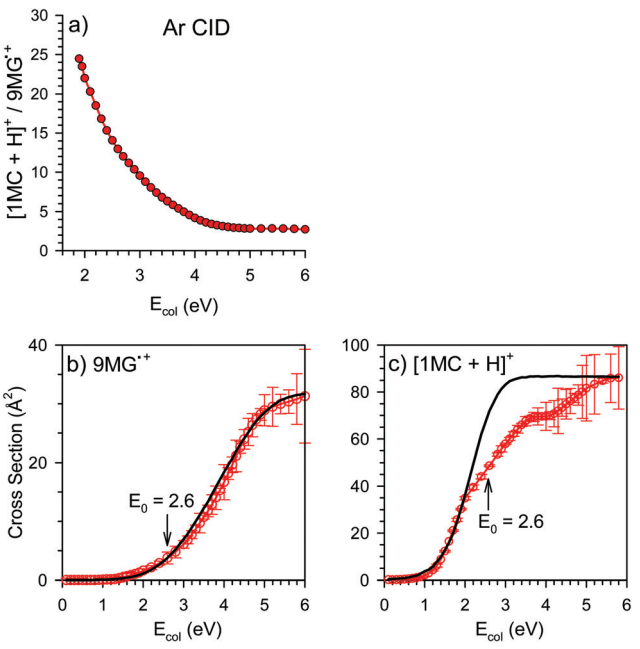

Fig. 4 CID results of $[9MG{\cdot}1MC]^{\bullet+}$ with Ar. (a) Product ion branching ratios as a function of E_{col}, and (b and c) product cross sections of $9MG^{\bullet+}$ and $[1MC + H]^{+}$ where circled points are experimental data and black curves are LOC fits as discussed in the text.

We also note that there is a glaring discrepancy between the fit and the experimental cross section of $[1MC + H]^{+}$ in Fig. 4c. This discrepancy can be rationalized as follows: CID produced a large fraction of sideway-scattered product ions. Compared to those in the collisions with Xe at the same E_{col}, the E_{lab} and thus the speed of the sideway-scattered product ions in the collisions with Ar are significantly higher, making these ions difficult to collect (particularly at high E_{col}) even using an ion guide.[61] Because of the inefficient $T \rightarrow E_{internal}$ transfer and the product ion collection problem in the Ar CID, we have chosen to only use the Xe CID results for kinetics analysis to eliminate artifact.

Statistical PES *vs.* non-statistical kinetics of $[9MG{\cdot}1MC]^{\bullet+}$. Fig. 5 represents the reaction PES for $[9MG{\cdot}1MC]^{\bullet+}$ calculated at the ωB97XD/6-311++G(d,p) level of theory, where the reactant $9MG^{\bullet+}{\cdot}1MC$ was located at zero potential energy. Fig. 5a shows PT between $9MG^{\bullet+}{\cdot}1MC$ and $[9MG - H_{N1}]^{\bullet}{\cdot}[1MC + H_{N3'}]^{+}$ and their respective dissociation asymptotes; and Fig. 5b shows HT4′ between $9MG^{\bullet+}{\cdot}1MC$ and $[9MG + H_{O6}]^{+}{\cdot}[1MC - H_{N4'}]^{\bullet}$ and the dissociation of the latter to $[9MG + H_{O6}]^{+} + [1MC - H_{N4'}]^{\bullet}$. We were not able to converge a TS structure for HT4′. The barrier height for TS_HT4′ was estimated from a relaxed PES scan along the HT4′ reaction coordinate.

The potential energies of base-pair conformers, their interconversion barriers and dissociation thresholds are the most

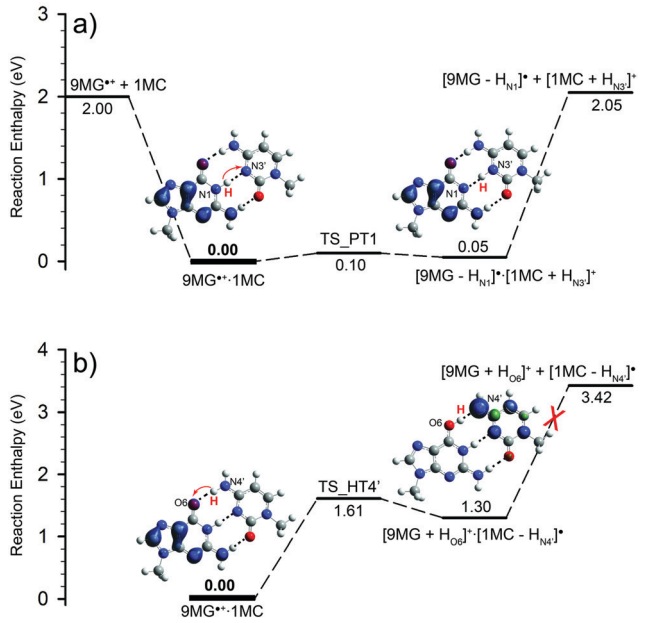

Fig. 5 PES for intra-base-pair PT1 and HT4′ in $[9MG{\cdot}1MC]^{\bullet+}$ and subsequent dissociation. Contour plots on GaussView structures illustrate spin densities. Reaction enthalpies were evaluated at ωB97XD/6-311++G(d,p), including thermal corrections at 298 K.

important quantities in examining base-pair reaction kinetics. Therefore, these values were re-calculated and validated at different levels of theory and using a wide range of basis sets, including ωB97XD/aug-cc-PVQZ, B3LYP/aug-cc-PVQZ, RI-MP2/aug-cc-pVTZ and DLPNO-CCSD(T)/aug-cc-pVTZ. The results are compiled in Table 1, with an overall good agreement.

Among the different theories, DLPNO-CCSD(T)/aug-cc-pVTZ may be considered as a reference. However, the DLPNO-CCSD(T)-calculated energy of $[9MG{+}H_{O6}]^{+}{\cdot}[1MC - H_{N4'}]^{\bullet}$ is suspiciously high; as a result, the dissociation energy of $[9MG + H_{O6}]^{+}{\cdot}[1MC - H_{N4'}]^{\bullet}$ to $[9MG + H_{O6}]^{+} + [1MC - H_{N4'}]^{\bullet}$ is only 0.55 eV. This unrealistically low dissociation energy casts doubt on DLPNO-CCSD(T) for this structure. On the other hand, the ωB97XD/6-311++G(d,p)-calculated energies not only agree well with DLPNO-CCSD(T) for most species (with the differences <0.05 eV), but provide a reasonable PES for the dissociation of $[9MG + H_{O6}]^{+}{\cdot}[1MC - H_{N4'}]^{\bullet}$ to $[9MG + H_{O6}]^{+} + [1MC - H_{N4'}]^{\bullet}$. Furthermore, the ωB97XD/6-311++G(d,p)-calculated dissociation energies best match the Xe-induced CID experimental data (within 0.05 eV). On the basis of both theoretical and experimental benchmarking, we chose to adopt the ωB97XD/6-311++G(d,p) energies in the PES. Note that TS and product energies for reactions (3) and (4) are the most important energies for the following kinetics analysis. As ωB97XD and DLPNO-CCSD(T) produced nearly identical energies for these species, it is assured that the kinetics analysis results are not affected by computational levels of theory.

According to the electron spin densities (shown as contours superimposed on GaussView structures in Fig. 5), the unpaired electron in both $9MG^{\bullet+}{\cdot}1MC$ and $[9MG - H_{N1}]^{\bullet}{\cdot}[1MC + H_{N3'}]^{+}$ is delocalized among the N3, C5 and C8 of the 9MG moiety. In contrast, the unpaired electron in $[9MG + H_{O6}]^{+}{\cdot}[1MC - H_{N4'}]^{\bullet}$ shifts to the N4 of 1MC. As a result, the formation energy of $[9MG + H_{O6}]^{+}{\cdot}[1MC - H_{N4'}]^{\bullet}$ and its dissociation threshold are 1.3–1.4 eV higher than those of $9MG^{\bullet+}{\cdot}1MC$, rendering this structure being insignificant in the reactant ion beam. This is consistent with the experiment where no product ions of $[9MG + H]^{+}$ (m/z 166) were observed.

The PES calculations have shown that $9MG^{\bullet+}{\cdot}1MC$ is slightly more stable than $[9MG - H_{N1}]^{\bullet}{\cdot}[1MC + H_{N3'}]^{+}$, and the two have very similar dissociation thresholds. On the other hand, the dissociation products of $[9MG - H]^{\bullet}{\cdot}[1MC + H]^{+}$ dominated in the CID experiments. The branching ratio of $[1MC + H]^{+}/9MG^{\bullet+}$ rises up to 12 at E_{col} = 1.8 eV and 1.3 at E_{col} = 6.0 eV in the Xe CID.

To illustrate the extent of non-statistical CID, we have predicted what the product distributions would be if the base pair dissociates statistically. To calculate the statistical product branching between $9MG^{\bullet+}$ and $[1MC + H]^{+}$, it is necessary to assume something about the relative formation efficiencies of $9MG^{\bullet+}{\cdot}1MC$ and $[9MG - H]^{\bullet}{\cdot}[1MC + H]^{+}$ during collisional activation. For this purpose, we calculated the equilibrium constant K_{PT} for $9MG^{\bullet+}{\cdot}1MC \rightleftharpoons [9MG - H]^{\bullet}{\cdot}[1MC + H]^{+}$, which is equivalent to the ratio of densities of states in the two conformers. The value of K_{PT} is E_{col}-dependent and varies from 0.42 at 0.5 eV, to 1.24 at 2 eV and 1.97 at 6 eV, *i.e.* the PT structure is becoming favorable with increasing E_{col}.

The RRKM branching ratio of $[1MC + H]^{+}/9MG^{\bullet+}$ is given by $K_{PT} \times \frac{k_{diss}([9MG - H]^{\bullet}[1MC + H]^{+})}{k_{diss}(9MG^{\bullet+}{\cdot}1MC)}$ where $k_{diss}([9MG - H]^{\bullet}{\cdot}[1MC + H]^{+})$ and $k_{diss}(9MG^{\bullet+}{\cdot}1MC)$ are the RRKM dissociation

Table 1 Comparison of PES energies (ΔH at 298 K, eV) of $[9MG{\cdot}1MC]^{\bullet+}$ at different levels of theory

Species	ωB97XD/ 6-311++G(d,p)	ωB97XD/ aug-cc-pVQZ	B3LYP/ aug-cc-pVQZ	RI-MP2/ aug-cc-pVTZ	DLPNO-CCSD(T)/ aug-cc-pVTZ
$9MG^{\bullet+}{\cdot}1MC$	0.0	0.0	0.0	0.0	0.0
$9MG^{\bullet+}$ + 1MC	2.00	1.92	1.75	2.12	1.96
TS_PT1	0.10	0.12	0.11	0.06	0.12
$[9MG - H_{N1}]^{\bullet}{\cdot}[1MC + H_{N3'}]^{+}$	0.05	0.06	0.05	0.04	0.07
$[9MG - H_{N1}]^{\bullet}$ + $[1MC + H_{N3'}]^{+}$	2.05	1.99	1.81	2.33	2.02
TS_HT4′	1.61	—	—	—	—
$[9MG + H_{O6}]^{+}{\cdot}[1MC - H_{N4'}]^{\bullet}$	1.30	1.32	1.22	2.57	2.66
$[9MG + H_{O6}]^{+}$ + $[1MC - H_{N4'}]^{\bullet}$	3.42	3.31	3.07	3.52	3.21

rate constants for the respective conformers (see eqn (2)). As there are no reverse barriers for base-pair dissociation, vibrational frequencies and moments of inertia appropriate to the dissociation TSs had to be assumed for the k_{diss} calculation. We first adopted orbiting TSs[67] for base-pair dissociation in which the TS frequencies are those of the products including their rotations. However, the resulting k_{diss} was unrealistically lower than the experimental ion detection time window, which was likely due to the ambiguities in the estimation of angular momenta in the orbiting TSs. We therefore estimated the TS properties on the basis of reactant frequencies using two different approaches.[67,68,99–101] At one extreme, the vibrational frequencies of the TSs are equal to those of the base pairs with the removal of only the symmetric stretching frequency of the WC hydrogen bonds (that corresponds to the base-pair dissociation reaction coordinate). These represent "tight" TSs for base-pair dissociation. At the other extreme, "loose" TSs were assumed for base-pair dissociation as follows. All of the frequencies that are partitioned into the dissociation products (which exhibit little changes in the dissociation and are referred to as conserved modes[102]) remain in the TSs. Of the six translational modes[102] which are lost upon dissociation, the symmetric stretching of the WC hydrogen bonds is removed, and the remaining five modes (corresponding to out-of-plane twisting, out-of-plane butterfly bending, anti-symmetric out-of-plane bending/step, in-plane bending/gearing and anti-symmetric stretching of the two bases with respect to each other) become the intermolecular motions of the dissociating base pair and their frequencies are scaled by a factor of 0.5 to reflect the "looseness" of TSs and the dissociation entropies. The choice of the scaling factor was based on literature work. The scaling factor was used by Armentrout's group to assign the transitional modes in dissociation of energized metal ion–ligand complex ML_x.[99–101] Dissociations of these ML_x complexes have no reverse activation barriers, and ion-dipole forces result in long range metal–ligand interactions. Therefore, the corresponding TSs must be truly "loose" TSs. The fact that the similarly scaled translational frequencies were successfully used to extract dissociation energies of ML_x suggests that this scaling factor yields appropriate "loose" TSs corresponding to weak associations of the products.

We have used both "tight" and "loose" TSs in the RRKM analysis. The two sets of RRKM results are plotted in Fig. 3b for comparison with the experiment. Clearly, the tightness of the TSs significantly affects reaction rates and thus the product branching ratios. The loose-TS-based RRKM predicts a branching ratio of $[1MC + H]^+/9MG^{\bullet+}$ around 0.1–0.2 in the low-E_{col} CID, increasing to 0.4 at high E_{col} (as the $[9MG - H]^{\bullet}\cdot[1MC + H]^+$ conformer is becoming more favorable at higher E_{col}). The tight-TS-based RRKM increases the $[1MC + H]^+/9MG^{\bullet+}$ ratio throughout the whole energy range and indeed approaches the experimental data at high energies. But neither of the two models is able to reproduce simultaneously both the predominance of $[1MC + H]^+$ at all energies and the decreasing trend of $[1MC + H]^+/9MG^{\bullet+}$ with increasing E_{col}.

Feketeová *et al.*[27] have reported CID of $[dG\cdot dC]^{\bullet+}$, in which the fragment ions presented a very statistical-like branching ratio of $[dC + H]^+/dG^{\bullet+}$ = 0.16. It is not surprising that contrasting CID product distributions were observed in $[dG\cdot dC]^{\bullet+}$ of Feketeová *et al. vs.* in the present $[9MG\cdot 1MC]^{\bullet+}$, as the two reaction systems and experimental conditions were different. First, dissociation of $[dG\cdot dC]^{\bullet+}$ was accompanied by the cleavage of sugar moieties from nucleosides, which may have interfered with the measurement of $[dC + H]^+/dG^{\bullet+}$. Secondly, CID of $[dG\cdot dC]^{\bullet+}$ was carried out *via* low-energy, multiple collisions with helium bath gas in an ion trap, whereas CID of $[9MG\cdot 1MC]^{\bullet+}$ was done *via* E_{col}-specific single collision with Xe (or Ar) in an ion guide. Compared to single ion-gas collision in the ion guide, multiple collisions in the ion trap facilitated energy transfer and energy randomization by means of long-time, sequential collisional activation which eventually led to statistical dissociation. In this sense, the ion trap experiment was more like thermal excitation. It is not unusual that different dissociation pathways and product branching were observed following thermal random excitation (*i.e.* after complete intramolecular vibrational relaxation) *vs.* short-time, non-random collisional activation, and the latter often produced nonstatistical fragmentation.[61,103–106] Our recent direct dynamics trajectory simulations of $[G\cdot C - H]^-$ suffice to demonstrate a representative case. Regardless of initial base-pair structures and populations in the trajectories, thermally excited $[G\cdot C - H]^-$ always followed statistical dissociation, whereas collisional activation of $[G\cdot C - H]^-$ resulted in strong non-statistical product distributions.

Note that another complexity of the $[9MG\cdot 1MC]^{\bullet+}$ chemistry concerns with the non-Aufbau behavior[107] of the conventional conformer, *i.e.*, its SOMO (singly occupied MO, located at 9MG) lies below its HOMO (centered at 1MC),[43] as illustrated by the molecular orbitals (MOs) in Scheme 1. Interestingly, a normal SOMO–HDMO (the highest doubly occupied MO, located at 1MC) order is restored in $[9MG - H]^{\bullet}\cdot[1MC + H]^+$. It is not clear whether the inverted *vs.* regular MOs have influenced base-pair dissociation. The fact that similar non-statistical CID was observed in the closed-shell $[G\cdot C - H]^-$ implies the non-Aufbau MOs are at least not essential to non-statistical kinetics.

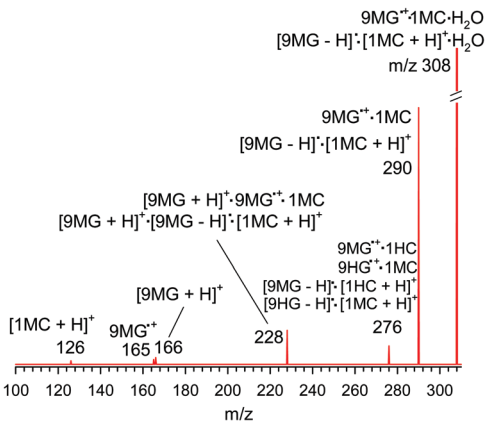

Fig. 6 CID product ion mass spectrum of $[9MG\cdot 1MC]^{\bullet+}\cdot H_2O$ + Xe measured at E_{col} = 4.0 eV.

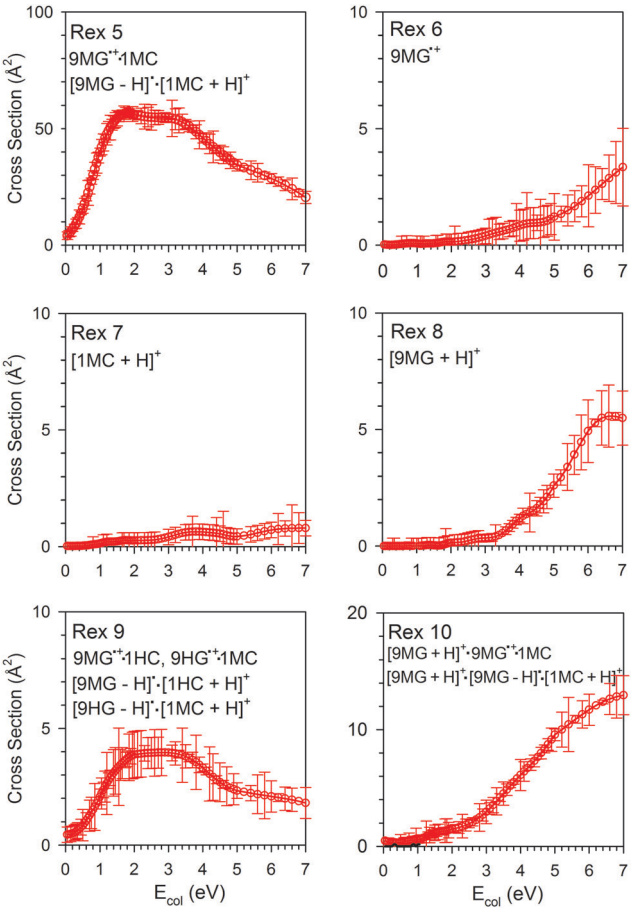

Fig. 7 Individual product ion cross sections in the collisions of [9MG·1MC]$^{\bullet+}$·H_2O with Xe.

3.2 Reactions of [9MG·1MC]$^{\bullet+}$·H_2O

Products and cross sections. A representative product ion mass spectrum of [9MG·1MC]$^{\bullet+}$·H_2O + Xe, taken at E_{col} = 4.0 eV, is shown in Fig. 6. Product ions were detected at six different *m*/*z*. Their assignments are given below, of which *m*/*z* 228 corresponds to doubly-charged dimer [9MG + H]$^{+}$·[9MG·1MC]$^{\bullet+}$ formed in reaction (10). The listed Δ*H*s for reactions (5)–(9) are from the ωB97XD/6-311++G(d,p) calculations.

$$9MG^{\bullet+}\cdot 1MC\cdot H_2O \rightarrow 9MG^{\bullet+}\cdot 1MC\ (m/z\ 290) + H_2O \quad \Delta H = 0.41\ eV \tag{5a}$$

$$[9MG - H_{N1}]^{\bullet}\cdot[1MC + H_{N3'}]^{+}\cdot H_2O \rightarrow [9MG - H_{N1}]^{\bullet}\cdot[1MC + H_{N3'}]^{+}\ (m/z\ 290) + H_2O \quad \Delta H = 0.48\ eV \tag{5b}$$

$$9MG^{\bullet+}\cdot 1MC\cdot H_2O \rightarrow 9MG^{\bullet+}\ (m/z\ 165) + 1MC + H_2O\ \Delta H = 2.41\ eV \tag{6}$$

$$[9MG - H_{N1}]^{\bullet}\cdot[1MC + H_{N3'}]^{+}\cdot H_2O \rightarrow [1MC + H_{N3'}]^{+}\ (m/z\ 126) + [9MG - H_{N1}]^{\bullet} + H_2O \quad \Delta H = 2.48\ eV \tag{7}$$

$$9MG^{\bullet+}\cdot 1MC\cdot H_2O \rightarrow [9MG + H_{O6}]^{+}\ (m/z\ 166) + [1MC - H_{N4'}]^{\bullet} + H_2O \quad \Delta H = 3.83\ eV \tag{8}$$

$$9MG^{\bullet+}\cdot 1MC\cdot H_2O \rightarrow 9MG^{\bullet+}\cdot 1HC\ (m/z\ 276) + CH_3OH\ \Delta H = 0.90\ eV \tag{9a}$$

$$9MG^{\bullet+}\cdot 1MC\cdot H_2O \rightarrow 9HG^{\bullet+}\cdot 1MC\ (m/z\ 276) + CH_3OH\ \Delta H = 1.01\ eV \tag{9b}$$

$$[9MG - H_{N1}]^{\bullet}\cdot[1MC + H_{N3'}]^{+}\cdot H_2O \rightarrow [9MG - H_{N1}]^{\bullet}\cdot[1HC + H_{N3'}]\ (m/z\ 276) + CH_3OH \quad \Delta H = 1.00\ eV \tag{9c}$$

$$[9MG - H_{N1}]^{\bullet}\cdot[1MC + H_{N3'}]^{+}\cdot H_2O \rightarrow [9HG - H_{N1}]^{\bullet}\cdot[1MC + H_{N3'}]^{+}\ (m/z\ 276) + CH_3OH \quad \Delta H = 1.06\ eV \tag{9d}$$

Table 2 Comparison of PES energies (Δ*H* at 298 K, eV) of [9MG·1MC]$^{\bullet+}$·H_2O at different levels of theory

Species	ωB97XD/ 6-311++G(d,p)	ωB97XD/ aug-cc-pVQZ	B3LYP/ aug-cc-pVQZ	RI-MP2/ aug-cc-pVTZ	DLPNO-CCSD(T)/ aug-cc-pVTZ
9MG$^{\bullet+}$·1MC·H_2O	0.0	0.0	0.0	0.0	0.0
9MG$^{\bullet+}$·1MC + H_2O	0.41	0.34	0.28	0.36	0.35
9MG$^{\bullet+}$ + 1MC + H_2O	2.41	2.26	2.03	2.49	2.32
TS_PT1·H_2O	0.06	0.09	0.08	0.03	0.08
[9MG − H_{N1}]$^{\bullet}$·[1MC + $H_{N3'}$]$^{+}$ ·H_2O	-0.02	-0.01	-0.01	-0.02	0.00
[9MG − H_{N1}]$^{\bullet}$·[1MC + $H_{N3'}$]$^{+}$ + H_2O	0.46	0.39	0.33	0.41	0.42
[9MG − H_{N1}]$^{\bullet}$ + [1MC + $H_{N3'}$]$^{+}$+ H_2O	2.46	2.32	2.09	2.70	2.37
TS_HT4′·H_2O	1.32	1.37	—	1.27	1.35
[9MG + H_{O6}]$^{+}$·[1MC − $H_{N4'}$]$^{\bullet}$·H_2O	1.22	1.25	1.17	2.63	2.73
[9MG + H_{O6}]$^{+}$ + [1MC − $H_{N4'}$]$^{\bullet}$ + H_2O	3.83	3.64	3.35	3.89	3.56
TS1·H_2O	3.70	3.77	3.51	3.86	3.78
9MG$^{\bullet+}$·1HC + CH_3OH	0.90	0.81	0.67	1.01	0.90
TS1_PT1	1.01	0.94	0.79	1.07	1.03
[9MG − H_{N1}]$^{\bullet}$·[1HC + $H_{N3'}$]$^{+}$ + CH_3OH	0.98	0.90	0.76	1.08	1.00
TS2·H_2O	3.55	3.61	3.40	3.61	3.63
9HG$^{\bullet+}$·1MC + CH_3OH	1.01	0.91	0.79	1.13	0.99
TS2_PT1	1.10	1.02	0.88	1.17	1.08
[9HG − H_{N1}]$^{\bullet}$·[1MC + $H_{N3'}$]$^{+}$ + CH_3OH	1.04	0.94	0.81	1.15	1.03

$$[9MG + H_{O6}]^+ + [9MG{\cdot}1MC]^{\bullet+} \rightarrow [9MG + H_{O6}]^+{\cdot}[9MG{\cdot}1MC]^{\bullet+} \quad (m/z\ 228) \qquad (10)$$

Fig. 7 depicts individual product ion cross sections in the E_{col} range of 0.1–7.0 eV. Our experiment was not able to distinguish different structures of the same m/z, therefore the cross sections of the same m/z (such as $9MG^{\bullet+}{\cdot}1MC$ and $[9MG - H]^{\bullet}{\cdot}[1MC + H]^+$) were lumped together. Due to complicated inter-channel competition and the mixed product structures at the same m/z, we did not attempt to extract threshold energies for individual reactions. But the product ion appearance energies agree qualitatively with the endothermic reaction enthalpies.

Formation of $9MG^{\bullet+}{\cdot}1MC$ and $[9MG - H]^{\bullet}{\cdot}[1MC + H]^+$ by water elimination (reactions (5a) and (5b)) represents the two energetically most favorable pathways and therefore accounts for the largest product cross sections. Among the products of reactions (6)–(8), $9MG^{\bullet+}$ and $[9MG + H]^+$ have comparable cross sections albeit that $[9MG + H]^+$ is slightly more favored at high E_{col}, and $[1MC + H]^+$ remains as a minor product throughout the whole E_{col} range. $9MG^{\bullet+}{\cdot}1HC$, $9HG^{\bullet+}{\cdot}1MC$ and their PT isomers, with the same m/z of 276, are formed by elimination of a methanol molecule from the monohydrated base-pair radical cations (reactions (9a)–(9d)). Methanol elimination represents the second major product channel in the middle range of E_{col}. Note that the cross sections of m/z 290 and m/z 276 demonstrate nearly identical E_{col} dependence: both channels increase with E_{col} and level off in the range of 2.0–3.5 eV before falling at higher E_{col}. The same E_{col} dependence implies that these product channels share the same rate-limiting step and/or a common intermediate. Most likely, $9MG^{\bullet+}{\cdot}1HC$, $9HG^{\bullet+}{\cdot}1MC$, $[9MG - H]^{\bullet}{\cdot}[1HC + H]^+$ and $[9HG - H]^{\bullet}{\cdot}[1MC + H]^+$ are the secondary reaction products of $9MG^{\bullet+}{\cdot}1MC$ and $[9MG - H]^{\bullet}{\cdot}[1MC + H]^+$ with water. Finally, as we have expected for a secondary combination reaction, the cross section of $[9MG + H]^+{\cdot}[9MG{\cdot}1MC]^{\bullet+}$ (reaction (10)) combines the E_{col} dependence of $[9MG{\cdot}1MC]^{\bullet+}$ and $[9MG + H]^+$.

In contrast to the numerous reactions occurring in the collisions of $[9MG{\cdot}1MC]^{\bullet+}{\cdot}H_2O$ with Xe, CID of $[9MG{\cdot}1MC]^{\bullet+}{\cdot}H_2O$ with Ar in the same E_{col} range produced only $[9MG{\cdot}1MC]^{\bullet+}$/$[9MG - H]^{\bullet}{\cdot}[1MC + H]^+$ (m/z 290, relative yield 90%) and $[9MG + H]^+{\cdot}9MG^{\bullet+}{\cdot}1MC$/$[9MG + H]^+{\cdot}[9MG - H]^{\bullet}{\cdot}[1MC + H]^+$ (m/z 228, relative yield 10%). This reinforces that Ar collisions are more short-lived and less efficient for promoting post-collision reactions.

Reaction PES due to hydration. The reactions of $[9MG{\cdot}1MC]^{\bullet+}{\cdot}H_2O$ were calculated at the different levels of theory. The results are compared in Table 2, with an overall good agreement. Fig. 8 summarizes the reaction PES for intra-base-pair PT1 and HT4′, water elimination, methanol elimination and base-pair dissociation that originate from the two lowest-energy monohydrates $[9MG - H]^{\bullet}{\cdot}[1MC + H]^+{\cdot}H_2O$ and $9MG^{\bullet+}{\cdot}1MC{\cdot}H_2O$. The energies in the figure are from the ωB97XD/6-311++G(d,p) calculations. The bold-labeled species represent the most probable product ion structures that were detected in the experiment.

Fig. 8a and b illustrate the intra-base-pair PT1 of $9MG^{\bullet+}{\cdot}1MC{\cdot}H_2O \rightleftharpoons [9MG - H_{N1}]^{\bullet}{\cdot}[1MC + H_{N3'}]^+{\cdot}H_2O$ *via* TS_PT1·H_2O and the intra-base-pair HT4′ of $9MG^{\bullet+}{\cdot}1MC{\cdot}H_2O \rightleftharpoons [9MG + H_{O6}]^+{\cdot}[1MC - H_{N4'}]^{\bullet}{\cdot}H_2O$ *via* TS_HT4′·H_2O, as well as the subsequent water elimination and base-pair dissociation. Except for water elimination, the reactions in Fig. 8a and b are the analogues of the reactions of dry $9MG^{\bullet+}{\cdot}1MC$ and $[9MG - H_{N1}]^{\bullet}{\cdot}[1MC + H_{N3'}]^+$. Note that TS_HT4′·$H_2O$ lies in energy 0.3 eV lower than its anhydrous analogue TS_HT4′, indicating that HT4′ becomes feasible upon hydration. This is

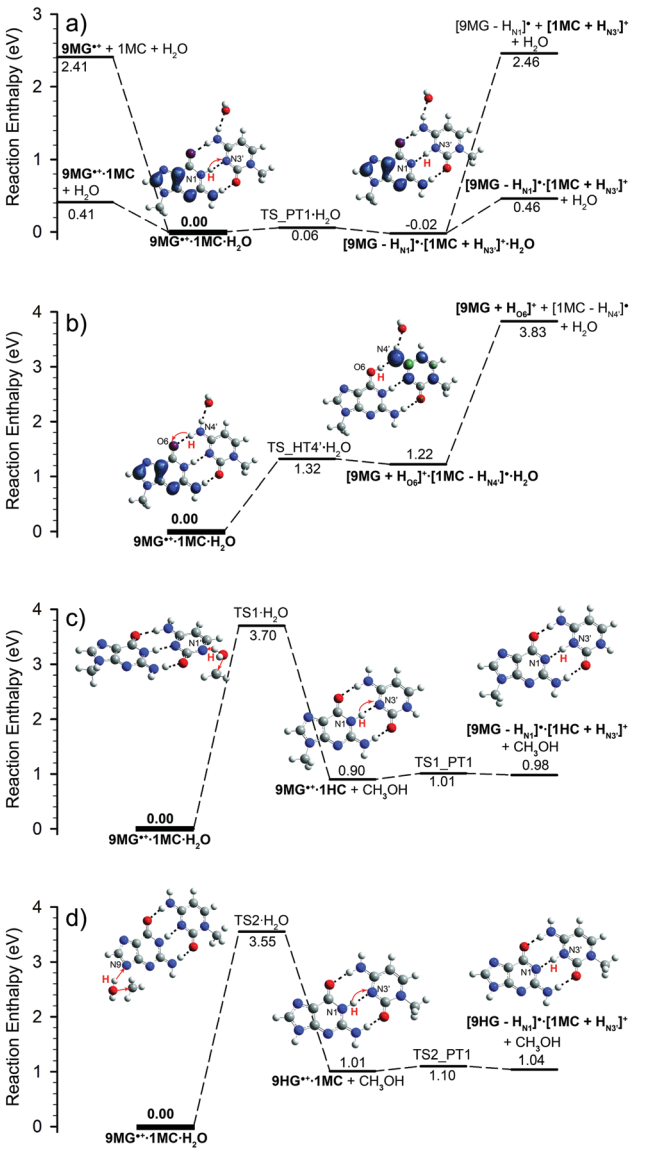

Fig. 8 Reaction PES for $[9MG{\cdot}1MC]^{\bullet+}{\cdot}H_2O$: (a) intra-base-pair PT1 and subsequent dissociation, (b) intra-base-pair HT4′ and subsequent dissociation, and (c and d) methanol elimination and subsequent intra-base-pair PT1. Contour plots on GaussView structures illustrate spin densities. Bold-labeled species represent the most probable product ion structures which were detected in the experiment. Reaction enthalpies were evaluated at ωB97XD/6-311++G(d,p), including thermal corrections at 298 K.

evidenced by the detection of its signature fragment ion $[9MG + H]^+$ (*m*/*z* 166) in the CID of $[9MG{\cdot}1MC]^{\bullet+}{\cdot}H_2O$.

Fig. 8c represents chemical reactions within $9MG^{\bullet+}{\cdot}1MC{\cdot}H_2O$. Upon collisional activation, the water ligand attacks the CH_3 group of 1MC *via* TS1·H_2O to form $9MG^{\bullet+}{\cdot}1HC + CH_3OH$ (reaction (9a)). The nascent $9MG^{\bullet+}{\cdot}1HC$ may interconvert to its PT counterpart $[9MG - H_{N1}]^{\bullet}{\cdot}[1HC + H_{N3'}]^+$ *via* TS1_PT1. Fig. 8d shows an alternative pathway for methanol elimination, in which $9HG^{\bullet+}{\cdot}1MC$ is produced by the attack of water on the CH_3 group of 9MG *via* TS2·H_2O (reaction (9b)) and converts to $[9HG - H_{N1}]^{\bullet}{\cdot}[1MC + H_{N3'}]^+$ *via* TS2_PT1 afterwards. The methanol elimination reactions presented in Fig. 8c and d are both originating from the conventional $9MG^{\bullet+}{\cdot}1MC{\cdot}H_2O$ conformer. Similar reactions may occur in $[9MG - H_{N1}]^{\bullet}{\cdot}[1MC + H_{N3'}]^{+}{\cdot}H_2O$ (reaction (9c) and (9d)). In the latter case, the barrier TS1·H_2O leading to $[9MG - H_{N1}]^{\bullet}{\cdot}[1HC + H_{N3'}]^+ + CH_3OH$ is lower by 0.22 eV, whereas the barrier TS2·H_2O leading to $[9HG - H_{N1}]^{\bullet}{\cdot}[1MC + H_{N3}']^+ + CH_3OH$ is higher by 0.04 eV than the corrsponding TSs in reaction (9a) and (9b).

Note that the barriers for methanol elimination were calculated to be 3.5 eV or higher for both $9MG^{\bullet+}{\cdot}1MC{\cdot}H_2O$ and $[9MG - H_{N1}]^{\bullet}{\cdot}[1MC + H_{N3'}]^{+}{\cdot}H_2O$. On the other hand, the product ion cross section for methanol elimination has an appearance energy that is comparable to that of $[9MG{\cdot}1MC]^{\bullet+}$/$[9MG - H]^{\bullet}{\cdot}[1MC + H]^+$. This leads us to further believe that methanol elimination should be more appropriately described as a secondary reaction between $[9MG{\cdot}1MC]^{\bullet+}$ (or $[9MG - H]^{\bullet}{\cdot}[1MC + H]^+$) and the dissociating water ligand that is still wandering around the base pair.

4. Conclusions

The present work has combined the guided-ion-beam mass spectrometric measurements of the collision-induced dissociation of $[9MG{\cdot}1MC]^{\bullet+}$ (both in the absence and the presence of a water ligand) with the dissection of reaction potential energy surfaces at the ωB97XD, B3LYP, RI-MP2, and DLPNO-CCSD(T) levels of theory. $[9MG{\cdot}1MC]^{\bullet+}$ has low-energy-barrier intra-base-pair proton transfer which leads to the formation of a major, conventional conformer $9MG^{\bullet+}{\cdot}1MC$ and a minor, proton-transferred conformer $[9MG - H]^{\bullet}{\cdot}[1MC + H]^+$. However, in contrast to what would be expected from a statistical base-pair dissociation reaction, $[1MC + H]^+$ which was generated from the dissociation of $[9MG - H]^{\bullet}{\cdot}[1MC + H]^+$ dominated the CID product ions of $[9MG{\cdot}1MC]^{\bullet+}$ at all collision energies; whereas $9MG^{\bullet+}$ generated from the dissociation of $9MG^{\bullet+}{\cdot}1MC$ remained as a minor product. It was also found that hydration of $[9MG{\cdot}1MC]^{\bullet+}$ by even a single water dramatically changed base-pair reactions and subsequent dissociation. Two new reactions (hydrogen transfer from 1MC to $9MG^{\bullet+}$ and the reaction of the water ligand with the methyl group in 9MG or 1MC) were detected in $[9MG{\cdot}1MC]^{\bullet+}{\cdot}H_2O$, which respectively led to the formation of $[9MG + H]^+$ and a methanol molecule in the dissociation products.

One of the most appealing findings in this work is the non-statistical base-pair dissociation. Understanding the origin of non-statistical kinetics and its entangling with intra-base pair reactions is challenging and thus has potential to probe the less intuitive aspects of guanine–cytosine base-pair chemistry. Similar non-statistical dissociation regime was observed in a previous CID experiment of deprotonated guanine–cytosine base pair, which raises a question of whether this is a general kinetics feature of guanine–cytosine base pair. We believe that non-statistical product distributions imply that either the formation of proton-transferred base-pair conformer was enhanced upon collisional activation or the proton-transferred base-pair conformer dissociated faster *via* a less tight TS than the conventional conformer. Rather than speculating, we defer the discussion of these intriguing issues until we complete an extensive direct dynamics trajectory study of the CID of $[9MG{\cdot}1MC]^{\bullet+}$ in different conformations, currently underway.

Conflicts of interest

There are no conflicts to declare.

Acknowledgements

This work was supported by National Science Foundation (Grant No. CHE 1856362). YS acknowledges CUNY Mina Rees Doctoral Dissertation Fellowship. The authors thank Professors Peter Armentrout (University of Utah) and Kent Ervin (University of Nevada, Reno) for providing the Crunch program.

References

1 S. Steenken and S. V. Jovanovic, *J. Am. Chem. Soc.*, 1997, **119**, 617–618.
2 C. J. Burrows and J. G. Muller, *Chem. Rev.*, 1998, **98**, 1109–1151.
3 J. Zhou, O. Kostko, C. Nicolas, X. Tang, L. Belau, M. S. de Vries and M. Ahmed, *J. Phys. Chem. A*, 2009, **113**, 4829–4832.
4 M. Schwell and M. Hochlaf, *Top. Curr. Chem.*, 2015, **355**, 155–208.
5 L. P. Candeias and S. Steenken, *J. Am. Chem. Soc.*, 1989, **111**, 1094–1099.
6 S. Steenken, *Chem. Rev.*, 1989, **89**, 503–520.
7 L. P. Candeias and S. Steenken, *J. Am. Chem. Soc.*, 1992, **114**, 699–704.
8 D. N. Nikogosyan, *Int. J. Radiat. Biol.*, 1990, **57**, 233–299.
9 E. D. A. Stemp and J. K. Barton, *Met. Ions Biol. Syst.*, 1996, **33**, 325–365.
10 I. Saito, T. Nakamura and K. Nakatani, *J. Am. Chem. Soc.*, 2000, **122**, 3001–3006.
11 H. H. Thorp, *Trends Biotechnol.*, 1998, **16**, 117–121.
12 C. Ribaut, G. Bordeau, P. Perio, K. Reybier, V. Sartor, O. Reynes, P.-L. Fabre and N. Chouini-Lalanne, *J. Phys. Chem. B*, 2014, **118**, 2360–2365.

13 H. Kasai, Z. Yamaizumi, M. Berger and J. Cadet, *J. Am. Chem. Soc.*, 1992, **114**, 9692–9694.
14 J. P. Hall, F. E. Poynton, P. M. Keane, S. P. Gurung, J. A. Brazier, D. J. Cardin, G. Winter, T. Gunnlaugsson, I. V. Sazanovich, M. Towrie, C. J. Cardin, J. M. Kelly and S. J. Quinn, *Nat. Chem.*, 2015, **7**, 961–967.
15 T. Caruso, M. Carotenuto, E. Vasca and A. Peluso, *J. Am. Chem. Soc.*, 2005, **127**, 15040–15041.
16 C. E. Crespo-Hernández, D. M. Close, L. Gorb and J. Leszczynski, *J. Phys. Chem. B*, 2007, **111**, 5386–5395.
17 M. Hutter and T. Clark, *J. Am. Chem. Soc.*, 1996, **118**, 7574–7577.
18 H. M. Jaeger and H. F. Schaefer, *J. Phys. Chem. B*, 2009, **113**, 8142–8148.
19 A. O. Colson, B. Besler and M. D. Sevilla, *J. Phys. Chem.*, 1992, **96**, 9787–9794.
20 F. D. Lewis, X. Liu, J. Liu, S. E. Miller, R. T. Hayes and M. R. Wasielewski, *Nature*, 2000, **406**, 51–53.
21 A. Adhikary, A. Kumar, D. Becker and M. D. Sevilla, *J. Phys. Chem. B*, 2006, **110**, 24171–24180.
22 K. Kobayashi and S. Tagawa, *J. Am. Chem. Soc.*, 2003, **125**, 10213–10218.
23 K. Kobayashi, R. Yamagami and S. Tagawa, *J. Phys. Chem. B*, 2008, **112**, 10752–10757.
24 J. A. Dean, *Lange's Handbook of Chemistry*, McGraw-Hill, New York, 15th edn, 1999.
25 A. W. Parker, C. Y. Lin, M. W. George, M. Towrie and M. K. Kuimova, *J. Phys. Chem. B*, 2010, **114**, 3660–3667.
26 Y. Rokhlenko, J. Cadet, N. E. Geacintov and V. Shafirovich, *J. Am. Chem. Soc.*, 2014, **136**, 5956–5962.
27 L. Feketeová, B. Chan, G. N. Khairallah, V. Steinmetz, P. Maitre, L. Radom and R. A. J. O'Hair, *J. Phys. Chem. Lett.*, 2017, **8**, 3159–3165.
28 P. O. Lowdin, *Rev. Mod. Phys.*, 1963, **35**, 724–732, discussion 732–723.
29 S. O. Kelley and J. K. Barton, *Science*, 1999, **283**, 375–381.
30 M. Ratner, *Nature*, 1999, **397**, 480–481.
31 M. G. Debije and W. A. Bernhard, *J. Phys. Chem. B*, 2000, **104**, 7845–7851.
32 S. C. Weatherly, I. V. Yang and H. H. Thorp, *J. Am. Chem. Soc.*, 2001, **123**, 1236–1237.
33 X. Li, Z. Cai and M. D. Sevilla, *J. Phys. Chem. B*, 2001, **105**, 10115–10123.
34 F. D. Lewis, R. L. Letsinger and M. R. Wasielewski, *Acc. Chem. Res.*, 2001, **34**, 159–170.
35 Q. Gu and D. T. Haynie, *Annu. Rev. Nano Res.*, 2008, **2**, 217–285.
36 K. Kawai, Y. Osakada and T. Majima, *ChemPhysChem*, 2009, **10**, 1766–1769.
37 J. Jie, K. Liu, L. Wu, H. Zhao, D. Song and H. Su, *Sci. Adv.*, 2017, **3**, e1700171.
38 K. Hildenbrand and D. Schulte-Frohlinde, *Free Radical Res. Commun.*, 1990, **11**, 195–206.
39 A. Adhikary, A. Kumar, S. A. Munafo, D. Khanduri and M. D. Sevilla, *Phys. Chem. Chem. Phys.*, 2010, **12**, 5353–5368.
40 A. Kumar and M. D. Sevilla, *J. Phys. Chem. B*, 2009, **113**, 11359–11361.
41 S. Steenken and J. Reynisson, *Phys. Chem. Chem. Phys.*, 2010, **12**, 9088–9093.
42 J. P. Ceron-Carrasco, A. Requena, E. A. Perpete, C. Michaux and D. Jacquemin, *J. Phys. Chem. B*, 2010, **114**, 13439–13445.
43 A. Kumar and M. D. Sevilla, *J. Phys. Chem. B*, 2014, **118**, 5453–5458.
44 R. G. Cooks, *J. Mass Spectrom.*, 1995, **30**, 1215–1221.
45 P. B. Armentrout, *J. Am. Soc. Mass Spectrom.*, 2002, **13**, 419–434.
46 Y. Seong, S. Y. Han, S.-C. Jo and H. B. Oh, *Mass Spectrom. Lett.*, 2011, **2**, 73–75.
47 B. Yang, R. R. Wu and M. T. Rodgers, *Anal. Chem.*, 2013, **85**, 11000–11006.
48 B. Yang and M. T. Rodgers, *J. Am. Chem. Soc.*, 2014, **136**, 282–290.
49 B. Yang, A. R. Moehlig, C. E. Frieler and M. T. Rodgers, *J. Phys. Chem. B*, 2015, **119**, 1857–1868.
50 B. Yang and M. T. Rodgers, *J. Am. Soc. Mass Spectrom.*, 2015, **26**, 1394–1403.
51 B. Yang, R. R. Wu and M. T. Rodgers, *J. Am. Soc. Mass Spectrom.*, 2015, **26**, 1469–1482.
52 W. Lu and J. Liu, *Phys. Chem. Chem. Phys.*, 2016, **18**, 32222–32237.
53 J. J. Park, C. S. Lee and S. Y. Han, *J. Am. Soc. Mass Spectrom.*, 2018, **29**, 2368–2379.
54 J. Liu, *Phys. Chem. Chem. Phys.*, 2017, **19**, 30616–30626.
55 Y. Fang and J. Liu, *J. Phys. Chem. A*, 2009, **113**, 11250–11261.
56 P. Cheng and D. K. Bohme, *J. Phys. Chem. B*, 2007, **111**, 11075–11082.
57 A. N. Krutchinsky, I. V. Chernushevich, V. L. Spicer, W. Ens and K. G. Standing, *J. Am. Soc. Mass Spectrom.*, 1998, **9**, 569–579.
58 C. Rebick and R. D. Levine, *J. Chem. Phys.*, 1973, **58**, 3942–3952.
59 R. D. Levine and R. B. Bernstein, *Molecular Reaction Dynamics and Chemical Reactivity*, Oxford University Press, New York, 1987.
60 P. B. Armentrout, *Int. J. Mass Spectrom.*, 2000, **200**, 219–241.
61 J. Liu, B. van Devener and S. L. Anderson, *J. Chem. Phys.*, 2002, **116**, 5530–5543.
62 K. M. Ervin and P. B. Armentrout, *J. Chem. Phys.*, 1985, **83**, 166–189.
63 M. E. Weber, J. L. Elkind and P. B. Armentrout, *J. Chem. Phys.*, 1986, **84**, 1521–1529.
64 R. H. Schultz, K. C. Crellin and P. B. Armentrout, *J. Am. Chem. Soc.*, 1991, **113**, 8590–8601.
65 N. F. Dalleska, K. Honma, L. S. Sunderlin and P. B. Armentrout, *J. Am. Chem. Soc.*, 1994, **116**, 3519–3528.
66 A. A. Shvartsburg, K. M. Ervin and J. H. Frederick, *J. Chem. Phys.*, 1996, **104**, 8458–8469.
67 M. T. Rodgers, K. M. Ervin and P. B. Armentrout, *J. Chem. Phys.*, 1997, **106**, 4499–4508.
68 M. T. Rodgers and P. B. Armentrout, *J. Chem. Phys.*, 1998, **109**, 1787–1800.
69 V. F. DeTuri and K. M. Ervin, *J. Phys. Chem. A*, 1999, **103**, 6911–6920.

70 C. Iceman and P. B. Armentrout, *Int. J. Mass Spectrom.*, 2003, **222**, 329–349.
71 W. J. Chesnavich and M. T. Bowers, *J. Phys. Chem.*, 1979, **83**, 900–905.
72 K. M. Ervin, *Int. J. Mass Spectrom.*, 1999, **185–187**, 343–350.
73 H. Koizumi and P. B. Armentrout, *J. Chem. Phys.*, 2003, **119**, 12819–12829.
74 H. Koizumi, F. Muntean and P. B. Armentrout, *J. Chem. Phys.*, 2004, **120**, 756–766.
75 J. C. Amicangelo and P. B. Armentrout, *J. Phys. Chem. A*, 2004, **108**, 10698–10713.
76 P. B. Armentrout, *J. Chem. Phys.*, 2007, **126**, 234302.
77 P. B. Armentrout, K. M. Ervin and M. T. Rodgers, *J. Phys. Chem. A*, 2008, **112**, 10071–10085.
78 M. B. Sowa-Resat, P. A. Hintz and S. L. Anderson, *J. Phys. Chem.*, 1995, **99**, 10736–10741.
79 R. A. Marcus, *J. Chem. Phys.*, 1952, **20**, 359–364.
80 J.-D. Chai and M. Head-Gordon, *Phys. Chem. Chem. Phys.*, 2008, **10**, 6615–6620.
81 M. J. Frisch, G. W. Trucks, H. B. Schlegel, G. E. Scuseria, M. A. Robb, J. R. Cheeseman, G. Scalmani, V. Barone, B. Mennucci, G. A. Petersson, H. Nakatsuji, M. Caricato, X. Li, H. P. Hratchian, A. F. Izmaylov, J. Bloino, G. Zheng, J. L. Sonnenberg, M. Hada, M. Ehara, K. Toyota, R. Fukuda, J. Hasegawa, M. Ishida, T. Nakajima, Y. Honda, O. Kitao, H. Nakai, T. Vreven, J. A. Montgomery Jr., J. E. Peralta, F. Ogliaro, M. Bearpark, J. J. Heyd, E. Brothers, K. N. Kudin, V. N. Staroverov, T. Keith, R. Kobayashi, J. Normand, K. Raghavachari, A. Rendell, J. C. Burant, S. S. Iyengar, J. Tomasi, M. Cossi, N. Rega, J. M. Millam, M. Klene, J. E. Knox, J. B. Cross, V. Bakken, C. Adamo, J. Jaramillo, R. Gomperts, R. E. Stratmann, O. Yazyev, A. J. Austin, R. Cammi, C. Pomelli, J. W. Ochterski, R. L. Martin, K. Morokuma, V. G. Zakrzewski, G. A. Voth, P. Salvador, J. J. Dannenberg, S. Dapprich, A. D. Daniels, O. Farkas, J. B. Foresman, J. V. Ortiz, J. Cioslowski and D. J. Fox, *Gaussian 09, Revision D.01*, Gaussian, Inc, Wallingford, CT, 2013.
82 F. B. van Duijneveldt, J. G. C. M. van Duijneveldt-van de Rijdt and J. H. van Lenthe, *Chem. Rev.*, 1994, **94**, 1873–1885.
83 F. Weigend, M. Haser, H. Patzelt and R. Ahlrichs, *Chem. Phys. Lett.*, 1998, **294**, 143–152.
84 P. Jurecka, P. Nachtigall and P. Hobza, *Phys. Chem. Chem. Phys.*, 2001, **3**, 4578–4582.
85 D. G. Liakos, M. Sparta, M. K. Kesharwani, J. M. L. Martin and F. Neese, *J. Chem. Theory Comput.*, 2015, **11**, 1525–1539.
86 F. Neese, *WIREs Comput. Mol. Sci.*, 2018, **8**, e1327.
87 I. M. Alecu, J. Zheng, Y. Zhao and D. G. Truhlar, *J. Chem. Theory Comput.*, 2010, **6**, 2872–2887.
88 T. Baer and W. L. Hase, *Unimolecular reaction dynamics: Theory and experiments*, Oxford University Press, New York, 1996.
89 W. L. Hase, *Acc. Chem. Res.*, 1998, **31**, 659–665.
90 K. Fukui, *J. Phys. Chem.*, 1970, **74**, 461–463.
91 L. Zhu and W. L. Hase, *Chem. Phys. Lett.*, 1990, **175**, 117–124.
92 K. K. Baldridge, M. S. Gordon, R. Steckler and D. G. Truhlar, *J. Phys. Chem.*, 1989, **93**, 5107–5119.
93 W. L. Hase, K. Bolton, P. de Sainte Claire, R. J. Duchovic, X. Hu, A. Komornicki, G. Li, K. Lim, D. Lu, G. H. Peslherbe, K. Song, K. N. Swamy, S. R. Vande Linde, A. Varandas, H. Wang and R. J. Wolf, *VENUS 99: A General Chemical Dynamics Computer Program*, Texas Tech University Lubbock, TX, 1999.
94 X. Hu, W. L. Hase and T. Pirraglia, *J. Comput. Chem.*, 1991, **12**, 1014–1024.
95 L. Zhu and W. L. Hase, *A general RRKM program (QCPE 644), Quantum chemistry program exchange*, Chemistry Department, University of Indiana, Bloomington, 1993.
96 J. Bordas-Nagy and K. R. Jennings, *Int. J. Mass Spectrom. Ion Processes*, 1990, **100**, 105–131.
97 P. B. Armentrout, *J. Anal. At. Spectrom.*, 2004, **19**, 571–580.
98 J. Liu, B. Uselman, J. Boyle and S. L. Anderson, *J. Chem. Phys.*, 2006, **125**, 133115.
99 F. Meyer, F. A. Khan and P. B. Armentrout, *J. Am. Chem. Soc.*, 1995, **117**, 9740–9748.
100 M. B. More, E. D. Glendening, D. Ray, D. Feller and P. B. Armentrout, *J. Phys. Chem.*, 1996, **100**, 1605–1614.
101 D. Ray, D. Feller, M. B. More, E. D. Glendening and P. B. Armentrout, *J. Phys. Chem.*, 1996, **100**, 16116–16125.
102 S. J. Klippenstein, A. L. L. East and W. D. Allen, *J. Chem. Phys.*, 1994, **101**, 9198–9201.
103 P. T. Fenn, Y. J. Chen, S. Stimson and C. Y. Ng, *J. Phys. Chem. A*, 1997, **101**, 6513–6522.
104 J. Liu, K. Song, W. L. Hase and S. L. Anderson, *J. Chem. Phys.*, 2003, **119**, 3040–3050.
105 E. Martínez-Núñez, S. A. Vázquez, F. J. Aoiz and J. F. Castillo, *J. Phys. Chem. A*, 2006, **110**, 1225–1231.
106 Z. Homayoon, S. Pratihar, E. Dratz, R. Snider, R. Spezia, G. L. Barnes, V. Macaluso, A. Martin Somer and W. L. Hase, *J. Phys. Chem. A*, 2016, **120**, 8211–8227.
107 G. Gryn'ova, D. L. Marshall, S. J. Blanksby and M. L. Coote, *Nat. Chem.*, 2013, **5**, 474–481.

